MOUTH-LIKE CRACKING IN A HIGH-STRENGTH MULTIPHASE STEEL AND ITS RELATIONSHIP TO FRACTURE TOUGHNESS

XUAN WANG[1], JICHENG GAO[1], YUN HANG[1], YI ZHENG[1], DEREK O. NORTHWOOD[2] & CHENG LIU[1]
[1]School of Mechanical Engineering, Yangzhou University, People's Republic of China
[2]Mechanical, Auto and Materials Engineering, University of Windsor, Canada

ABSTRACT

The effect of microstructure on crack growth behaviour in steels has always been a subject of considerable research interest. Based on a quenching and partitioning process (Q&P), and the transformation of a nano-scaled bainite in advanced high-strength steels, a novel quenching-partitioning-austempering process (Q-P-A) has been developed for manufacturing a multiphase microstructure in a medium carbon steel (55Mn2SiCr). The processing sequence consists of the following steps: austenitizing at 900°C for 0.5 h; controlled quenching and cooling to 200°C, i.e. slightly below Ms (the start temperature for martensite transformation) for 5 s; austempering at 170°C for 5 min; up-heating to 250°C for 120 min; final air cooling to room temperature. An ultimate tensile strength (UTS) above 2 GPa, as well as an acceptable elongation of 3%, is obtained due to a multiphase formation comprising prior martensite (PM), bainitic ferrite (BF), retained austenite (RA) and nano-scaled structure ((BF + $RA_{(+C)}$)nano). Mouth-like cracks are observed on the fracture surface and the crack arrest behavior is investigated. When a microstructural cluster with (BF + $RA_{(+C)}$)nano fully covered PM is formed, a mouth-like crack can be formed and a superior crack resistance can be obtained. The crack initiates from the PM boundary and propagates along the interface between the PM and (BF + $RA_{(+C)}$)nano over a distance of a few millimeters and before being arrested in the (BF + $RA_{(+C)}$)nano. This behaviour is mainly attributed to the uniform distribution of film RA and needle BF with nano-level spacing in the (BF + RA)nano. The stress concentration energy at the crack tip can be absorbed by the martensitic transformation of the film RA. The results are important when designing a multiphase microstructure for a commercial high-strength steel.

Keywords: high tensile strength, mouth-like crack, quenching-partitioning-austempering process, nano-scaled structure, crack initiation and propagation.

1 INTRODUCTION

Advanced high-strength steels (AHSS) have been widely investigated due to their excellent strength, good ductility and high strength to weight ratio as majority of engineering designs require structural materials to have high strength and fracture toughness while minimizing weight. The latest generation of AHSS, also called the third generation of AHSS, produced by quenching and partitioning (Q&P) process, can provide a better strength and ductility combination compared to the first generation, while with a lower cost than the second generation [1]. The Q&P process was proposed by Speer et al. [2] in 2003, and consisted of an interrupted quenching process between the martensite-start temperature (Ms) and the martensite-finish temperature (Mf) after full austenitization or intercritical annealing. Accordingly, new AHSS have been developed based on the phase transition mechanism in the Q&P process for improved properties [3].

Nowadays, among the various competitive strategies to obtain AHSS, a low temperature isothermal treatment for producing a super bainitic steel has received considerable attention [4]. Such steels have excellent mechanical properties, as well as an affordable price. This is mainly due to the nano-scaled microstructures comprising bainitic ferrite (BF) sheaves and carbon-enriched retained austenite (RA) trapped between BF laths. However,

WIT Transactions on Engineering Sciences, Vol 133, © 2021 WIT Press
www.witpress.com, ISSN 1743-3533 (on-line)
doi:10.2495/MC210011

the long isothermal treatment time, over 60 days, would be totally unacceptable for commercial manufacture. Navarro-López et al. [5] have pointed out that prior martensite (PM), which is formed during quenching step in the process of Q&P treatment, could accelerate the bainite transformation kinetics by creating potential nucleation sites at the martensite-austenite interfaces, in addition to the austenite boundaries. Generally, a multiphase microstructure comprising PM, bainitic ferrite (BF) plus retained austenite (RA) is considered as an attractive microstructure for the third generation of advanced high-strength steels [6]–[9].

The influence of microstructure on crack propagation behavior in the high-performance steels has been an important research field [10]–[12]. Recently, Zhao et al. [13] investigated the fatigue failure mechanism of a multiphase steel. They found that the crack initiation site within a multiphase structure was the dominant factor influencing the high fatigue strength. Yajima et al. [14] in their research on the crack nucleation mechanism of austempered ductile iron during tensile deformation, reported that the cracks could benefit to the stress-induced martensitic transformation. Traditionally, it is believed that cracks are harmful to the properties of steel, especially for AHSS which requires not only high tensile strength but also excellent ductility [15]–[17].

In this paper, the cracks morphologies are studied in a medium carbon steel (55Mn2SiCr) that was heat treated using a quenching-partitioning-austempering (Q-P-A) process, that was developed in-house. The relationship between the initiation and propagation of mouth-like cracks, the multiphase microstructure and the mechanical properties is discussed.

2 EXPERIMENTAL PROCEDURES

The investigated material was a 6 mm-thick, hot-rolled and normalized plate. The composition is given in Table 1. Ms point of the steel calculated using the MUCG83 thermodynamic model, is 207°C [18]. The shape and size of tensile sample is shown in Fig. 1, which is designed according to ASTM standard E8M [19]. The scheme of the applied heat treatments is presented in Fig. 2. The processing sequence consists of the following steps: austenitizing at 900°C for 0.5 h; controlled quenching and cooling to 200°C, i.e. slightly below Ms (the start temperature for martensite transformation) for 5 s; quenching at 170°C for 5 min; up-heating to 250°C for 30, 60, 120 and 240 min respectively; final air cooling to room temperature.

A surface layer of 0.35 mm-thickness for tensile samples was removed after heat treatment and the tensile test with a 100 kN load at a crosshead speed of 0.05 mm·min^{-1} was conducted on a DNS100 universal testing machine. A HR-150A Rockwell hardness tester was used for hardness measurement with a 150 kg load and 120° diamond cone indenter. Microhardness tests were made by a Sinowon HV-1000A machine with a diamond square cone indenter and a load of 0.98 N.

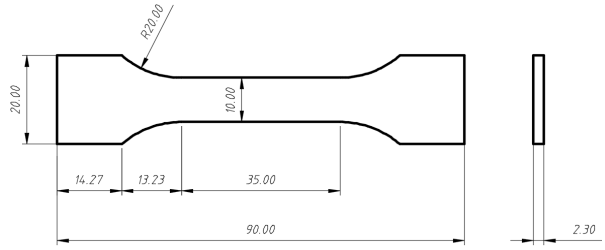

Figure 1: Geometry and dimensions (unit: mm) of tensile specimen.

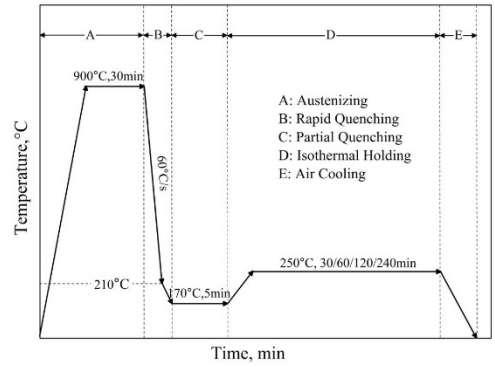

Figure 2: Schematic for heat treatment process.

Table 1: Chemical composition of sample (wt. %).

C	Si	Mn	Cr	V	Mo	P	S	Fe
0.57	1.50	1.83	0.83	0.03	0.01	0.01	0.007	Bal.

After being ground, polished and etched in 2% Nital solution, the microstructural characteristics of the samples were examined using optical microscopy (OM, LEICA GQ-300). The fracture surfaces of all samples were observed on a XL30-ESEM scanning electron microscope (SEM). Quantitative analysis of the microstructures were made using Image-Pro Plus 6.0 software.

3 RESULTS AND DISCUSSION

3.1 Microstructure

OM micrographs of the as-received samples after hot-rolling and normalizing are presented in Fig. 3. The microstructure is mainly composed of pearlite and ferrite. The dark gray area in Fig. 3(a) is pearlite and the white area is ferrite. From the grey area in Fig. 3(b), the lamella structure of pearlite can be clearly observed.

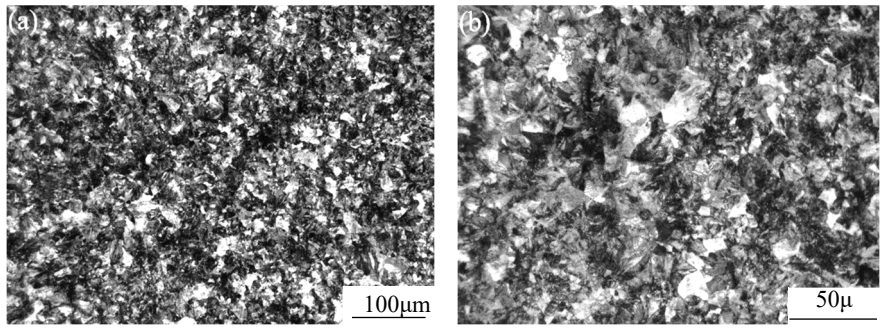

Figure 3: OM micrographs of as-received steel. (a) Low magnification; and (b) High magnification.

Fig. 4 shows that the OM micrographs of the samples after austempering at 250°C for various times. Typical microstructures consist of prior martensite (PM), bainitic ferrite (BF) and retained austenite (RA). With increasing tempering time, the content of PM does not appear to change, and the amount of BF increases. RA exists in the form of blocks or films. With increasing the tempering time, the content of blocky RA decreases, but the film RA increases. Corresponding SEM micrographs are presented in Fig. 5. PM is dark, which has obvious boundaries with the surrounding phases, and its internal substructure can be observed. RA appears as a grey phase with an overall content tending to decrease with time. Fig. 6 shows the detailed microstructure of the sample after austempering at 250°C for 60 min. Carbide precipitation is evident in the PM.

3.2 Mechanical properties

Fig. 7 summarises the hardness and microhardness results for samples austempered for 30, 60, 120 and 240 min at 250°C. The hardness (HRC) shows a small decrease, 60 to 55 HRC, with increasing austempering time. The microhardness measurements allowed us to probe the hardness of the constituent phases (RA, BF, PM). The RA showed the largest hardness decrease of the constituent phases, decreasing from 800 HV for 30 min austempering, to 600–650 HV after 60 min austempering. The PM hardness decreased from 770 HV after 30 min austempering to about 700 HV after 120 min austempering. The BF hardness remained approximately constant at a level of 670 to 700 HV.

Figs 8 and 9 summarise the mechanical properties (YS, TS, % elongation). The YS and TS both increase with austempering time up to an austempering time of 120 min. Austempering for 240 min produces a substantive reduction in both YS and TS. The % elongation initially increases with austempering time from 30 min to 60 min, but then

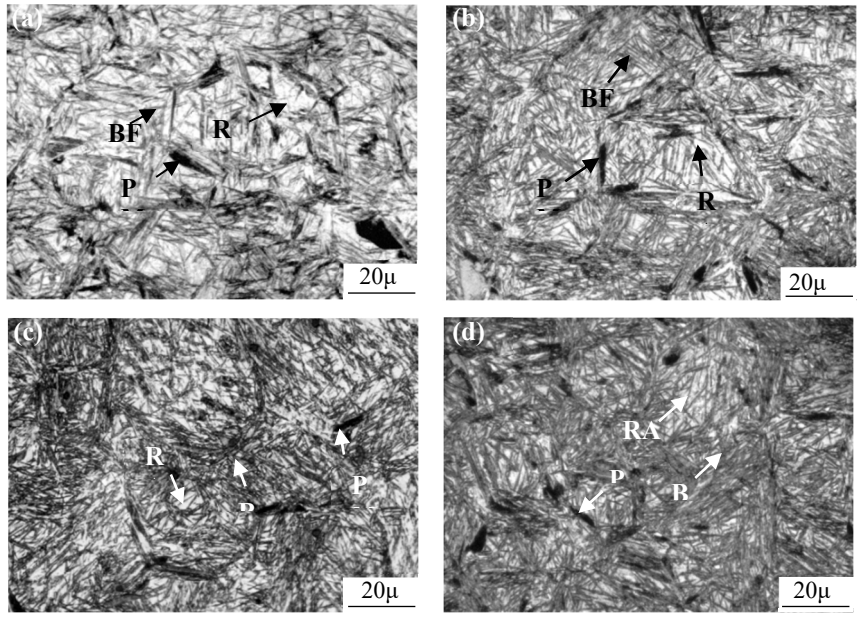

Figure 4: OM micrographs of samples after austempering at 250°C for (a) 30 min; (b) 60 min; (c) 120 min; and (d) 240 min.

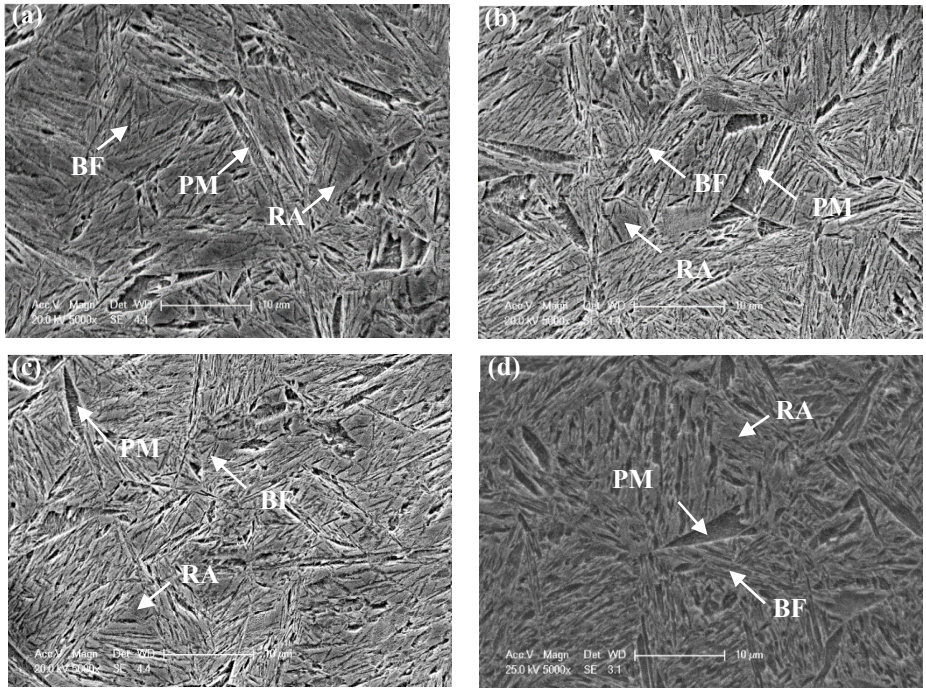

Figure 5: SEM micrographs of samples after austempering at 250°C for (a) 30 min; (b) 60 min; (c) 120 min and (d) 240 min.

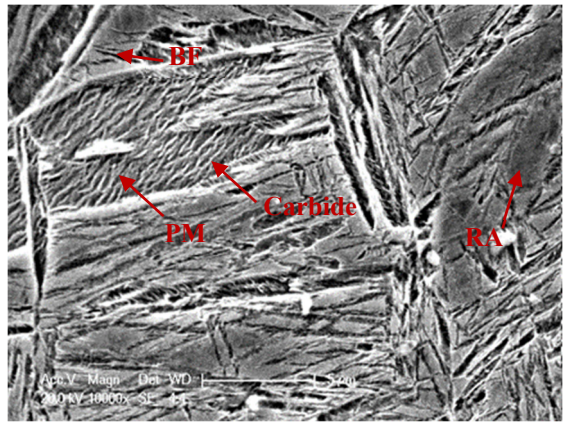

Figure 6: High magnification SEM micrograph of sample at 250°C for 60 min.

decreases with a further increase in austempering time. The optimum mechanical properties are produced by austempering at 250°C for 120 min: YS 1,684 MPa; TS 2,030 MPa; 3% elongation.

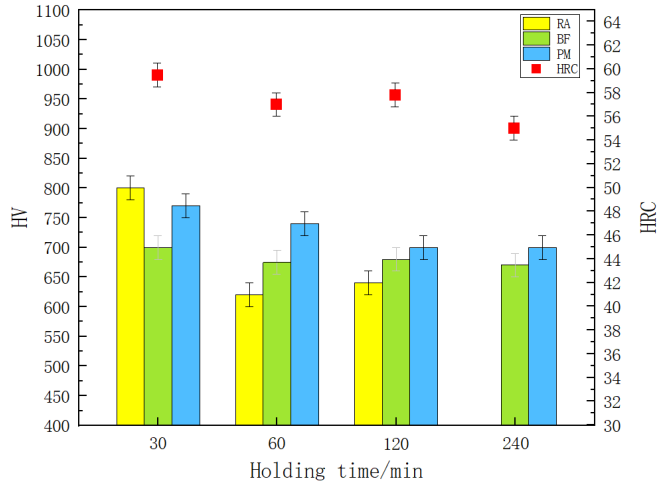

Figure 7: Hardness of samples after austempering at 250°C for different times.

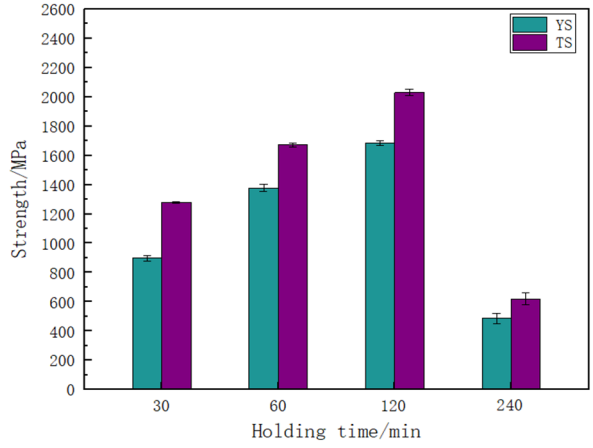

Figure 8: Mechanical properties of samples after austempering at 250°C for different times.

3.3 Mouth-like cracking and mechanisms of failure

The fracture surfaces of samples austempered for various times are shown in Figs 10–13. In the sample austempered at 250°C for 30 min, a ductile and brittle fracture mode is observed (see Fig. 10). The red circle indicated in Fig. 10(a) is in the sheared lip zone, which is mainly composed of small and uniform dimples. Nearby is a small crack, shown by the green rectangle area in Fig. 10(a). This crack has flat upper and lower surfaces, and looks like a mouth with two open corners (crack tips). It is about 30 μm long and 3.0 μm wide. Mixed brittle and ductile fracture of the upper face and a cleavage characteristic in the lower face of the mouth-like crack were observed. A similar crack was found in the sample austempered

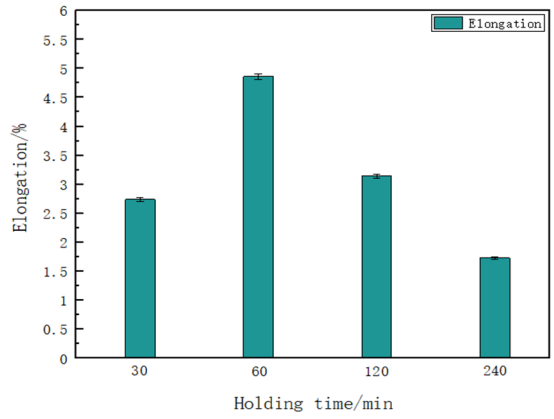

Figure 9: Elongation of samples after austempering at 250°C for different times.

for 60 min, Fig. 11. It had a length of about 20 μm and a width of 4.0 μm. At a high magnification, Fig. 11(b) and (c), it was evident that the sample austempered for 60 min had more dimples on both fracture surfaces than that for 30 min (Fig. 10(c)).

It can be seen from Fig. 12 that the morphology of the mouth-like crack observed in austempered sample for 120 min at 250°C is different from those shown in Figs 10 and 11 in two respects. First, the upper or lower surface of mouth-like crack is full of small, uniform dimples, indicating a ductile failure mode. Second, the two mouth corners of the crack are closed, forming a crack closure loop. The crack length was about 75 μm and the crack width was 15 μm. Fig. 13 illustrates the morphology of a large crack in the sample austempered for

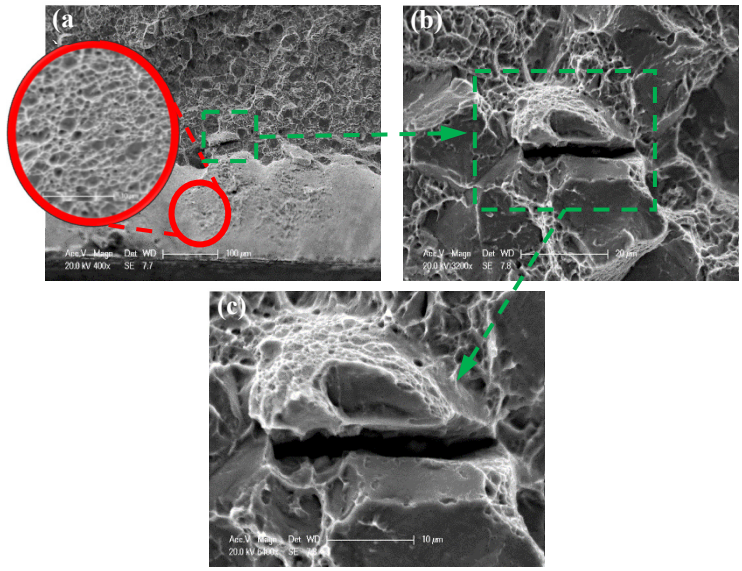

Figure 10: SEM micrographs of tensile fracture of sample austempered at 250°C for 30 min. (a) 400×; (b) 3,200×; and (c) 6,400×.

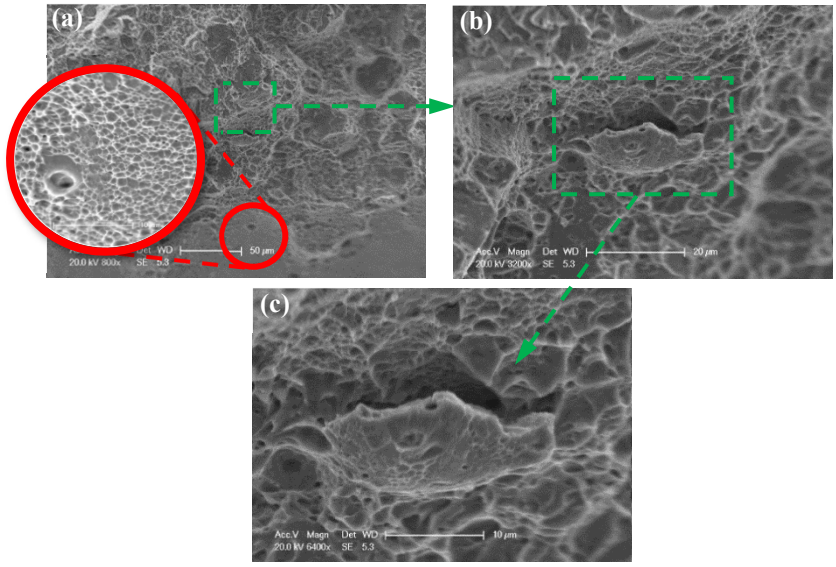

Figure 11: SEM micrographs of tensile fracture of sample austempered at 250°C for 60 min. (a) 800×; (b) 3,200×; and (c) 6,400×.

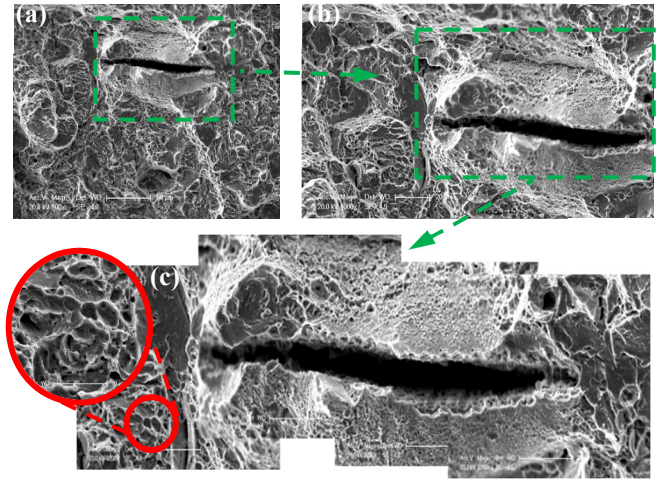

Figure 12: SEM micrographs of tensile fracture of sample at 250°C for 120 min. (a) 800×; (b) 1,600×; and (c) 3,200×.

240 min at 250°C, which is non-mouth-like and consisted of a main crack (100 μm long and 20 μm wide) and a secondary crack (50 μm long and 1.0 μm wide). The fracture morphology on both sides of the main crack is quite different. The crack upper side is dominated by dimples with different scales and depths while the lower side indicates a cleavage fracture mode.

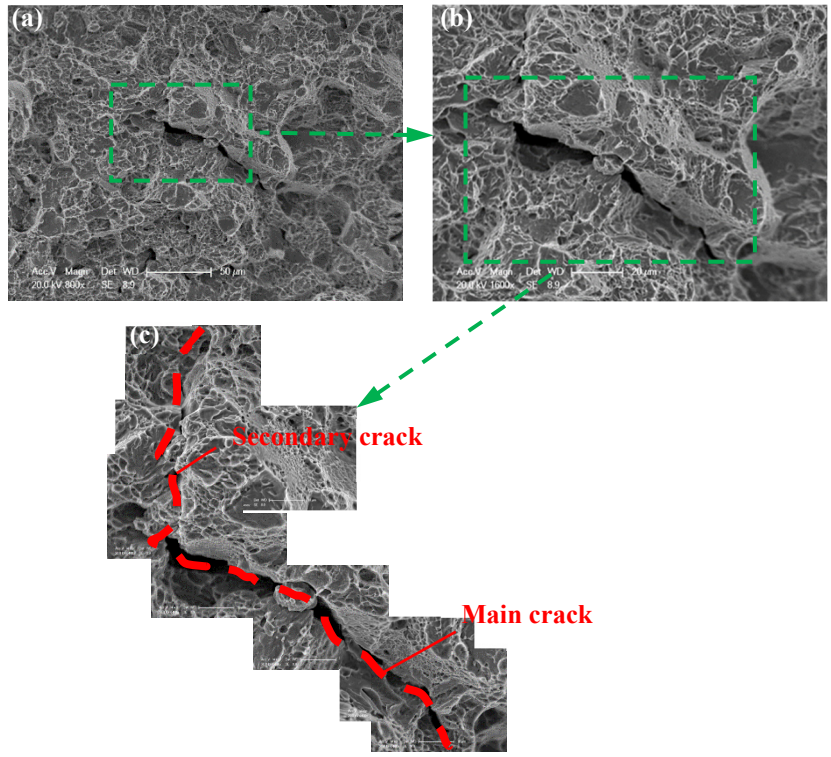

Figure 13: SEM micrographs of tensile fracture of sample austempered at 250°C for 240 min. (a) 800×; (b) 1,600×; and (c) 6,400×.

A schematic of the phase transformation during Q-P-A process is presented in Fig. 14. The main purpose of the rapid cooling (see Fig. 2(b)) is to avoid the formation of non-martensite phases such as pearlite and ferrite. About 30% prior martensite (PM) can be produced from austenite by partial quenching to 180°C (below the Ms), based on the calculation in ref. [20] and our previous experimental results [21] (see Fig. 15(a)). When the sample is austempered at 250°C, the supersaturated carbon atoms in the PM partially precipitate within the martensitic lath and partially partition through the phase boundaries to the austenite (A), due to a high Si content of the 55Mn2SiCr alloy. With respect to the partially tempered PM, it is easy for BF to nucleate at a local carbon-depleted area along the boundary between PM and A. Because of a relatively low carbon diffusion rate at 250°C and an uneven carbon distribution on the phase interface, nano-scaled BF laths are formed, interwoven with A films. When the austempering time increases, the BF growth occurs by more carbon atoms diffusing from BF into A. Thus, a carbon concentration in A increases to become $A_{(+C)}$, and finally $RA_{(+C)}$ at room temperature. That is, a unique microstructural cluster is formed by the Q-P-A process based on the carbon diffusion characteristics of PM, which is composed of a nano structure (BF + $RA_{(+C)}$) nucleating around a PM ((BF + $RA_{(+C)}$)nano).

The formation of a mouth-like crack is mainly related to the nano-scaled microstructural cluster. Fig. 15 is a schematic diagram of mouth-like crack initiation and propagation. When

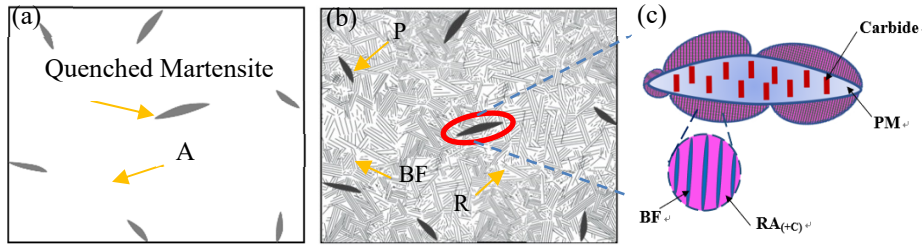

Figure 14: Schematic illustration of phase transformation during Q-P-A process.

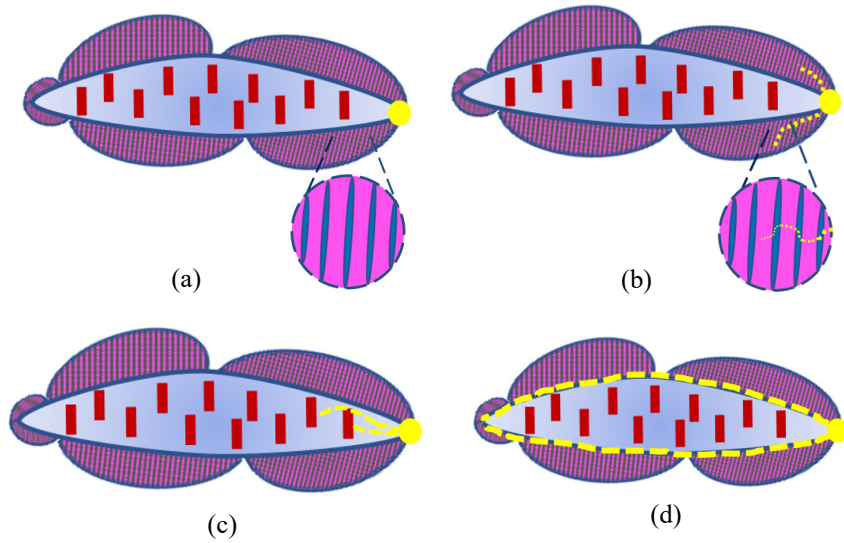

Figure 15: Schematic of mouth-like crack formation. (a) Crack initiation at tip of PM; (b) Crack propagation through (BF + RA(+C)) nanostructure surrounding the PM; (c) Crack propagation into the PM; and (d) Crack propagation along the PM-(BF + RA(+C)) nano) interface.

local plastic deformation occurs under tensile loading, the boundary between the PM and (BF + $RA_{(+C)}$) is an area where the stress concentration is high due to non-uniform deformation of the various phases, and can therefore initiate micro-cracks. Fig. 15 shows that there are three ways for crack propagation after forming on the boundary within nano-scaled structure cluster. It may propagate into the PM and its propagation is stopped or lessened when it meets the carbide phase in the martensitic lath (see Fig. 15(c)). Or it may enter into the (BF + $RA_{(+C)}$)nano around the PM. The crack propagating orientation will be changed by the influence of the fine laminated structure (see Fig. 15(b)) and finally stop. It has been reported that the multiphase nano-laminate microstructure can not only deflect the crack during propagation, but also be arrested by a metastable multiphase martensite-austenite transformation-induced plasticity (TRIP) effect [22]. The stress concentration energy at the crack tip can be absorbed by the martensitic transformation of the film RA.

Also, the micro-crack can propagate preferentially along the PM-(BF + $RA_{(+C)}$)nano interface (see Fig. 15(d)), since the BF nucleation occurs close to rather than at the interface [23]. An extremely small austenite area with an inhomogeneous carbon concentration can provide a channel for crack growth. If the PM is fully covered by the (BF + $RA_{(+C)}$)nano, the crack will be arrested with the structure cluster when the crack reaches the boundaries of (BF + $RA_{(+C)}$) nano, resulting in a mouth-like crack with closed corners. Thus, the tensile strength is increased. If not, a mouth-like crack with open corners is formed, which is attributed to a relatively lower mechanical property. This is supported by the mechanical property data in Figs 7 and 9. The poor mechanical properties of the sample austempered for 240 min are probably due to carbide precipitation from austenite and BF. Thus, the carefully designed multiphase microstructure has been changed, which is detrimental to the mechanical properties. Further investigation is required by XRD and TEM.

4 CONCLUSIONS

A multiphase high-strength steel is obtained by using a novel quenching-partitioning-austempering process (Q-P-A). The resultant microstructure consists of prior martensite (PM), bainitic ferrite (BF), retained austenite (RA) and (BF + $RA_{(+C)}$)nano. Mouth-like cracks are observed on the fracture surfaces of tensile test samples austempered at 250°C for 30, 60 and 120 min during tensile tests. The morphology of mouth-like cracks can influence the mechanical property. A mouth-like crack with closed corners, formed when the (BF + RA(+C))nano nucleation occurs fully around the PM, produces the optimum combination of mechanical properties.

REFERENCES

[1] Bleck, W., Brühl, F., Ma, Y. & Sasse, C., Materials and processes for the third-generation advanced high-strength steels. *Berg- und hüttenmännische Monatshefte*, **164**(11), pp. 466–474, 2019.

[2] Speer, J., Matlock, D.K., De Cooman, B.C. & Schroth, J.G., Carbon partitioning into austenite after martensitic transformation. *Acta Materialia*, **51**, pp. 2611–2622, 2003.

[3] Huyghe, P. et al., On the effect of Q&P processing on the stretch-flange-formability of 0.2C ultra-high strength steel sheets. *ISIJ International*, **58**(7), pp. 1341–1350, 2018.

[4] Avishan, B., Tavakolian, M. & Yazdani, S., Two-step austempering of high performance steel with nanoscale microstructure. *Materials Science & Engineering A*, **693**, pp. 178–185, 2017.

[5] Navarro-López, A., Sietsma, J., & Santofimia, M.J., Effect of prior athermal martensite on the isothermal transformation kinetics below Ms in a low-C high-Si steel. *Metallurgical and Materials Transactions A*, **47**, pp. 1028–1039, 2016.

[6] Diego-Calderón, I.D. et al., Effect of microstructure on fatigue behavior of advanced high strength steels produced by quenching and partitioning and the role of retained austenite. *Materials Science & Engineering A*, **641**, pp. 215–224, 2015.

[7] Amel-Farzad, H., Faridi, H.R., Rajabpour, F., Abolhasani, A., Kazemi, S. & Khaledzadeh, Y., Developing very hard nanostructured bainitic steel. *Materials Science and Engineering A*, **559**, pp. 68–73, 2013.

[8] Kang, J., Zhang, F.C., Yang, X.W., Lv, B. & Wu, K.M., Effect of tempering on the microstructure and mechanical properties of a medium carbon bainitic steel. *Materials Science and Engineering A*, **686**, pp. 150–159, 2017.

[9] Zhao, P., Zhang, B., Cheng, C., Misra, R.D.K., Gao, G. & Bai, B., The significance of ultrafine film-like retained austenite in governing very high cycle fatigue behavior in an ultrahigh-strength MN-SI-Cr-C steel. *Materials Science and Engineering: A*, **645**, pp. 116–121, 2015.
[10] Zhang, Z., Koyama, M., Wang, M.M., Tsuzaki, K., Tasan, C.C. & Noguchi, H., Effects of lamella size and connectivity on fatigue crack resistance of TRIP-maraging steel. *International Journal of Fatigue*, **100**, pp. 176–186, 2017.
[11] Koyama, M., Zhang, Z., Wang, M., Ponge, D., Raabe, D. & Tsuzaki, K., Bone-like crack resistance in hierarchical metastable nanolaminate steels. *Science*, **355**, pp. 1055–1057, 2017.
[12] Chai, G. & Zhou, N., Study of crack initiation or damage in very high cycle fatigue using ultrasonic fatigue test and microstructure analysis. *Ultrasonics*, **53**, pp. 1406–1411, 2013.
[13] Zhao, P. et al., Non-inclusion induced crack initiation in multiphase high-strength steel during very high cycle fatigue. *Materials Science & Engineering A*, **712**, pp. 406–413, 2018.
[14] Yajima, Z., Kishi, Y., Shimizu, K., Mochizuki, H. & Yoshida, T., Crack nucleation mechanism of austempered ductile iron during tensile deformation. *Materials Transactions*, **47**(1), pp. 82–89, 2006.
[15] Shiozawa, K., Morii, Y., Nishino, S. & Lu, L., Subsurface crack initiation and propagation mechanism in high-strength steel in a very high cycle fatigue regime. *International Journal of Fatigue*, **28**, pp. 1521–1532, 2006.
[16] Khan, M.K. & Wang, Q.Y., Investigation of crack initiation and propagation behavior of AISI 310 stainless steel up to very high cycle fatigue. *International Journal of Fatigue*, **54**, pp. 38–46, 2013.
[17] Chai, G., The formation of subsurface non-defect fatigue crack origins. *International Journal of Fatigue*, **28**, pp. 1533–1539, 2006.
[18] Peet, M. & Bhadeshia, H.K.D.H., www.msm.cam.ac.uk/map/steel/tar/mucg83.exe.
[19] ASTM Standard E8/E8M-16a, *Standard Test Methods for Tension Testing of Metallic Materials*. ASTM International: West Conshohocken, PA, 2016.
[20] Koistinen, D.P. & Marburger, R.E., A general equation prescribing the extent of the austenite-martensite transformation in pure iron-carbon alloys and plain carbon steels. *Acta Metallurgica*, **7**, pp. 59–60, 1959.
[21] Cui, X.X., Northwood, D.O. & Liu, C., Role of prior martensite in a 2.0 GPa multiple phase steel. *Steel Research International*, **89**(10), p. 1800207, 2018.
[22] Santofimia, M.J. & Zhao, L., Overview of mechanisms involved during the quenching and partitioning process in steels. *Metallurgical and Materials Transactions A*, **42**, pp. 3620–3626, 2011.
[23] Toji, Y., Matsuda, H. & Raabe, D., Effect of Si on the acceleration of bainite transformation by pre-existing martensite. *Acta Materialia*, **116**, pp. 250–262, 2016.